

# FAST GRAPH-BASED DENOISING FOR POINT CLOUD COLOR INFORMATION

Ryosuke Watanabe <sup>†,‡</sup>, Keisuke Nonaka <sup>‡</sup>, Eduardo Pavez <sup>†</sup>, Tatsuya Kobayashi <sup>‡</sup>, Antonio Ortega <sup>†</sup>

<sup>†</sup> University of Southern California, <sup>‡</sup> KDDI Research, Inc.

## ABSTRACT

Point clouds are utilized in various 3D applications such as cross-reality (XR) and realistic 3D displays. In some applications, e.g., for live streaming using a 3D point cloud, real-time point cloud denoising methods are required to enhance the visual quality. However, conventional high-precision denoising methods cannot be executed in real time for large-scale point clouds owing to the complexity of graph constructions with  $K$  nearest neighbors and noise level estimation. This paper proposes a fast graph-based denoising (FGBD) for a large-scale point cloud. First, high-speed graph construction is achieved by scanning a point cloud in various directions and searching adjacent neighborhoods on the scanning lines. Second, we propose a fast noise level estimation method using eigenvalues of the covariance matrix on a graph. Finally, we also propose a new low-cost filter selection method to enhance denoising accuracy to compensate for the degradation caused by the acceleration algorithms. In our experiments, we succeeded in reducing the processing time dramatically while maintaining accuracy relative to conventional denoising methods. Denoising was performed at 30fps, with frames containing approximately 1 million points.

**Index Terms**— point cloud denoising, fast graph construction, real-time denoising, noise estimation, graph signal processing

## 1. INTRODUCTION

Point clouds are utilized in a variety of 3D applications such as cross-reality (XR) [1] and holographic 3D displays [2]. In these applications, scanned point clouds, consisting of a collection of 3D coordinates and associated color signals, are often perturbed by noise caused by sensor measurement errors. Thus, point cloud denoising methods are important to improve the accuracy of downstream tasks such as object detection [3], action recognition [4], and point cloud compression [5]. In many applications, denoising must be executed in

real time. For example, in a point cloud streaming scenario for a 3D telepresence system, denoising is required just after scanning to reduce noise caused by a sensor, and after receiving data on the user side to suppress noise caused by compression errors. If a point cloud is scanned and transmitted in real time for 3D telepresence, denoising must be executed in real time.

Some methods have been proposed to reduce noise on point cloud geometry [6, 7, 8, 9, 10], while others focus on color denoising [11, 12, 13, 14, 15]. Since both geometry and color information directly affect visual quality, they are important to enhance the user experience in 3D applications. Though our proposal can be applied to both color and geometry denoising, here we focus on point cloud color denoising and leave geometry denoising for future work. Deep learning-based and graph-based approaches have been among the most widely studied techniques for point cloud color denoising in recent years. We focus on graph-based methods [12, 13, 14] because, unlike deep learning-based methods [11], training data are not required. Recent graph-based approaches include graph Laplacian regularization (GLR) [12], spectral graph wavelet-based color denoising (CD-SGW) [13], and 3-dimensional patch-based similarity (3DPBS) [14]. GLR [12] utilizes graph Laplacian regularization as a smoothness prior to achieve accurate color denoising. CD-SGW [13] utilizes BayesShrink [16], a popular wavelet shrinking technique for image denoising, to reduce the high-frequency wavelet components in the graph spectral domain. In 3DPBS [14], to improve the denoising accuracy, a graph construction method that is not susceptible to noise has been proposed. However, since detailed 3D models in these applications often result in large-scale point clouds with hundreds of thousands of points [17, 18], conventional denoising methods [12, 13, 14] cannot be performed in real time. This is due primarily to the large computation times required by  $K$  nearest neighbors (KNN) graph constructions in graph-based methods [12, 13, 14].

Many methods to speed up graph construction, in particular, KNN, have been proposed [19, 20, 21, 22, 23, 24]. Some of them [19, 20] work well for high-dimensional data but are less effective for 3D data such as point clouds. Although parallel computing methods with a GPU [21, 22] are proposed, the processing time is still large because they calculate distances between points by brute-force approach. To construct a graph from a point cloud, a neighbor search from each point is

Copyright © 2024 IEEE. Personal use of this material is permitted. Permission from IEEE must be obtained for all other uses, in any current or future media, including reprinting/republishing this material for advertising or promotional purposes, creating new collective works, for resale or redistribution to servers or lists, or reuse of any copyrighted component of this work in other work.

required to decide the connectivity. Fast methods build a data structure suitable for neighborhood search, e.g., kd-tree [23] or linear bounding volume hierarchy (LBVH) [24], in advance, speeding up the neighbor search process dramatically compared with the brute-force methods [21, 22]. These methods are most efficient when the data structures do not change. However, in point cloud video, a new data structure is needed for each frame, so these methods are not as advantageous.

The proposed method called fast graph-based denoising (FGBD) realizes real-time denoising for a large-scale point cloud. The starting point of FGBD is our recent research called 3DPBS [14], which is a high-precision and large-complexity color denoising method. Fig.1 describes that 3DPBS is composed of three major processes: 1) KNN-based graph construction, 2) low-pass filter selection based on an estimated noise level, and 3) low-pass filter execution on graph spectral domain. As discussed above, KNN graph construction has a large complexity. In addition, since the noise level is estimated by a conventional SGWT-based noise estimation method [13], the noise estimation process has significant complexity. Although noise estimation may not be required in all frames if there is no change in the noise level, it frequently changes in practice, e.g., noise caused by the scanning sensor’s heat. Thus, high-speed processing is desirable to respond quickly to the changes. Finally, though 3DPBS utilizes polynomial approximation in the low-pass filter execution process to represent flexible frequency response, the approximation has some complexity. The previous study [15] can solve the complexity of the low-pass filter execution. However, denoising accuracy is degraded. Our study, FGBD, solves these three major problems regarding complexity without significant denoising performance degradation compared with conventional accurate denoising methods.

Our paper’s contributions are as follows: 1) A **scan-line graph (SLG) construction** that does not require building a data structure in advance. 2) A fast and accurate **noise estimation using graph-based patches (NE-GBP)** based on principal component analysis (PCA) on a set of neighborhoods. 3) An accurate **filter selection with limited region (FSLR)** which improves low-pass filter selection scheme proposed by 3DPBS [14] with low-cost processing. The choice of low-pass filter’s frequency response is improved by not using some regions where the noise-free signals have high-frequency components (e.g., regions where a few sharp color changes).

While contributions 1) and 2) mainly focus on improving computation speed, contribution 3) is a proposal to improve denoising accuracy with a slight increase in processing time. In the experiments, FGBD is carried out with a single GPU based on NVIDIA CUDA implementation. We report that the processing of FGBD was 1500 times faster than

This work was supported by the Ministry of Internal Affairs and Communications (MIC) of Japan (Grant no. JPJ000595).

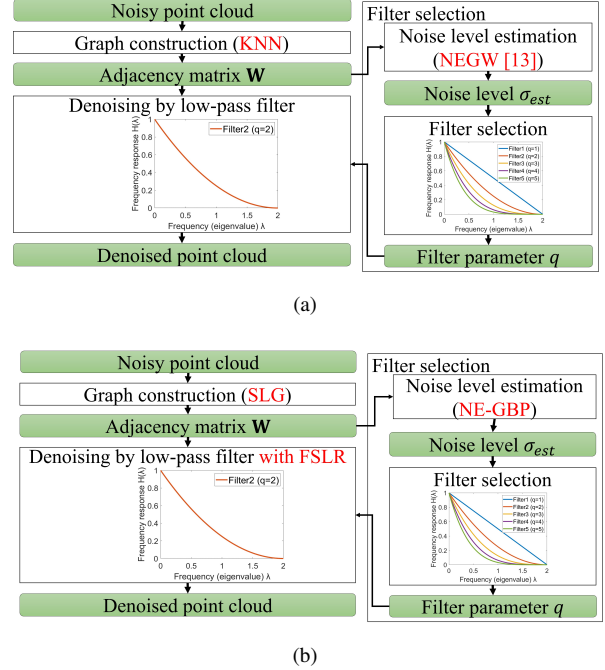


Fig. 1: Basic flow of (a) 3DPBS [14] and (b) FGBD (proposed).

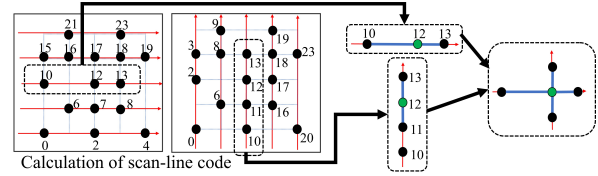


Fig. 2: Neighbor search on scan-line codes (Example of 2-D).

that of 3DPBS with 8iVFBv2 [17] and MVUB [18] datasets while maintaining the denoising accuracy. As a result, denoising was performed in real time at 30fps with a point cloud composed of around 1 million points. Note that our proposed methods, particularly SLG, can also be applied to accelerate geometry denoising using graph-based methods. Furthermore, SLG has the potential to contribute to speeding up not only denoising but also various applications that utilize a graph.

## 2. PROPOSED DENOISING METHOD

### 2.1. Overview of fast graph-based denoising (FGBD)

Fig.1 shows the overall calculation flow of the proposed method called FGBD, which includes the following 4 steps.

1. A graph is constructed from a noisy point cloud by using a scan-line graph (SLG).
2. Noise level  $\sigma_{est}$  is estimated by the method called noise estimation using graph-based patches (NE-GBP).

3. The parameter of a graph low-pass filter is determined by using filter selection with limited region (FSLR).
4. Color attributes are denoised using a vertex domain low-pass graph filter [15].

We explain steps 1 and 2 in Section 2.2 and Section 2.3, respectively. Finally, steps 3 and 4 are described in Section 2.4.

## 2.2. Graph construction based on SLG

We introduce a high-speed graph construction method called SLG. A graph is constructed from a given noisy point cloud  $P = \{p_i\}_{i=1}^N$ , where point  $p_i$  has coordinate  $\mathbf{g}_i \in \mathbb{R}^3$  and attribute signals  $\mathbf{f}_i \in \mathbb{R}^3$ . SLG assumes that the coordinate signals  $\mathbf{g}_i$  are quantized to integers with  $b$  bits. Since most point clouds in real-time applications go through voxelization, they have integer coordinates [5]. If they are represented by floating points, the coordinate signals  $\mathbf{g}_i$  are quantized to integers before starting the graph construction

Fig. 2 shows the graph construction process of SLG. First, a one-dimensional code (called scan-line code)  $C_{i,l}$ , where  $l$  indicates the index of a line, is calculated from  $\mathbf{g}_i$ . For example, scan-line codes calculated by raster scan are expressed by

$$C_{i,1} = 2^{2b} \mathbf{g}_{i,z} + 2^b \mathbf{g}_{i,y} + \mathbf{g}_{i,x}, \quad (1)$$

$$C_{i,2} = 2^{2b} \mathbf{g}_{i,x} + 2^b \mathbf{g}_{i,z} + \mathbf{g}_{i,y}, \quad (2)$$

$$C_{i,3} = 2^{2b} \mathbf{g}_{i,y} + 2^b \mathbf{g}_{i,x} + \mathbf{g}_{i,z}, \quad (3)$$

where  $\mathbf{g}_{i,x}$  shows the  $x$ -coordinate value of  $\mathbf{g}_i$ . Second, points are ordered based on each scan-line code  $C_{i,l}$  by a GPU-friendly sort algorithm, called radix sort [25]. Next, two consecutive points on the scan-line code are regarded as neighbors and connected in a graph. This process is carried out independently for each code. In other words, 6 neighborhoods ( $= 2$  neighbors  $\times 3$  codes) are obtained when we introduce 3 codes represented by (1), (2), and (3). Finally, after acquiring the connectivity by SLG, the adjacency matrix  $\mathbf{W} = \{w_{ij}\}$  is calculated by using the Gaussian kernel as follows.

$$w_{ij} = \exp\left(-\frac{(\mathbf{g}_i - \mathbf{g}_j)^2}{\sigma_g^2}\right). \quad (4)$$

If  $\sigma_g$  is very large (respectively small) relative to the numerator, all the weights become almost 1 (respectively 0). To avoid those two extreme cases,  $\sigma_g$  is computed as the average Euclidean distance between  $p_i$  and its neighbors. Note that when a raster scan is performed, a distant connection may occur when a scan line connects to the next line. In this case, the Euclidean distance becomes too large and the similarity is close to zero in  $\mathbf{W}$ . Thus, this connection does not cause an adverse effect.

Since neighbors can be obtained by only sorting, computing connectivity in a graph no longer requires many distance calculations or building a specific data structure such as

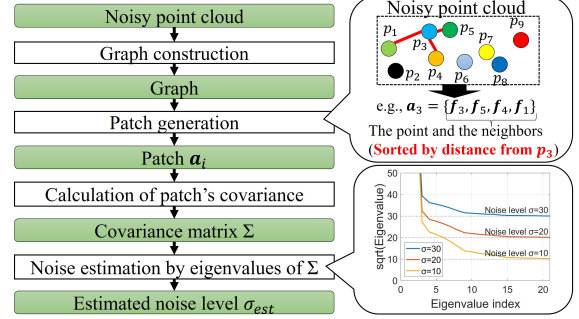


**Fig. 3:** Noise estimation using graph-based patches (NE-GBP)

kdtree. In our preliminary experiments, we tried other types of codes, e.g., Morton codes [5] and diagonal scan-lines instead of (1), (2), and (3). However, the three line-scan codes introduced above provide the best trade-off between accurate denoising and construction speed. Therefore,  $C_{i,1}, C_{i,2}$  and  $C_{i,3}$  are adopted in this paper.

## 2.3. Noise estimation using graph-based patches (NE-GBP)

The problem of noise estimation has been widely studied in conventional 2-D image processing. In particular, noise estimation methods using the covariance matrix of image patches achieve fast and accurate noise estimation results [26, 27, 28]. In these methods, after many small 2-D patches having the same size, e.g., blocks of  $8 \times 8$  pixels, are taken from an image by a raster scan, the eigenvalues of the covariance matrix of patches are calculated. Assuming that noise-free signals in small 2-D patches lie on a low-dimensional subspace, the noise variance can be estimated from the eigenvalues of principal components corresponding to higher frequencies that represent mostly noise. However, the application of noise estimation methods for image processing to point clouds is not straightforward because of the irregular point cloud geometry. NE-GBP utilizes the eigenvalues of the covariance matrix generated with small patches constructed with a graph. Fig. 3 shows the flow of NE-GBP.

First, a graph is constructed from a given noisy point cloud. Although arbitrary graph construction methods can be applied, here, SLG described in Section 2.2 is directly utilized.

Second, patches  $\mathbf{A} = \{\mathbf{a}_i\}_{i=1}^N \in \mathbb{R}^{D \times N}$  are constructed from the attribute signal of  $p_i$  and the neighbors from  $p_i$  where  $D$  is the number of signals in a patch. As shown in Fig. 3, to better capture the statistical properties of different patches in the covariance matrix construction, the order of entries in vectors representing each patch should be consistent. Specifically, for any given patch vector, the entries (i.e., the attributes of the nodes) are ordered based on increasing distances of nodes within the patch. Thus, the first entry of each vector is the attribute of the query point, followed by the closest neigh-

**Table 1:** Processing time [s] of 3DPBS and FGBD in each section. The GC, NE, and LF indicate “graph construction”, “noise estimation”, and “low-pass filter execution”, respectively. These figures are average times per frame for all the frames and noise levels.

Method	3DPBS		FGBD-CPU		FGBD-GPU	
	8i	MVUB	8i	MVUB	8i	MVUB
GC [s]	3.588	1.769	0.289	0.095	0.008	0.005
NE [s]	17.342	13.655	0.912	0.323	0.032	0.010
LF [s]	71.009	24.270	1.210	0.395	0.019	0.011
Total [s]	91.939	39.693	2.411	0.812	0.058	0.026

bor, and ending with the furthest neighbor. In sorted patches, the covariance matrix of patches  $\Sigma \in \mathbb{R}^{D \times D}$  is calculated as  $\Sigma = \frac{1}{N} \sum_{i=1}^N (\mathbf{a}_i - \boldsymbol{\mu})(\mathbf{a}_i - \boldsymbol{\mu})^T$  where  $\boldsymbol{\mu} = \frac{1}{N} \sum_{i=1}^N \mathbf{a}_i$  is the mean of all patches.

Next, the noise level  $\sigma_{\text{est}}$  is estimated by using eigenvalues  $\{\lambda_k\}_{k=1}^D$  ( $\lambda_1 \geq \lambda_2 \geq \dots \geq \lambda_D$ ) of the covariance matrix  $\Sigma$ . The original noise-free point cloud leads to patch covariance with eigenvalues that are close to zero for the subspace  $S_H = \{\lambda_k\}_{k=m+1}^D$ . Thus, for a point cloud with noisy attributes, we propose to estimate the noise variance from the eigenvalues of  $S_H$ . As derived theoretically in [27],  $m$  should be chosen such that  $\tau = \frac{1}{D-m+1} \sum_{k=m+1}^D \lambda_k > \text{median}(\{\lambda_k\}_{k=m+1}^D)$ . With this  $m$  the noise level is calculated as  $\sigma_{\text{est}} = \sqrt{\tau}$ .

#### 2.4. Filter selection and low-pass filter execution

In FGBD, the low-pass filter is applied as follows:

$$\mathbf{f}_{\text{out}} = (\mathbf{D}_g^{-1} \mathbf{W}_g)^q \mathbf{f}_{\text{in}}, \quad (5)$$

where  $\mathbf{f}_{\text{in}}$  and  $\mathbf{f}_{\text{out}}$  are input and denoised signals, respectively.  $q$  represents the number of iterations of the filtering. Here, the adjacency matrix with self-loops  $\mathbf{W}_g$  is defined as  $\mathbf{W}_g = \mathbf{D} + \mathbf{W}$  where  $\mathbf{D}$  is the degree matrix of  $\mathbf{W}$ , and  $\mathbf{D}_g$  is described as  $2\mathbf{D}$ . According to the discussion in the previous study [15], the spectral interpretation of (5) on the graph Fourier domain is described as  $h_q(\lambda_i) = (1 - \frac{1}{2}\lambda_i)^q$ . In 3DPBS, the parameter  $q$  is determined to satisfy the following condition based on  $\sigma_{\text{est}}$ :

$$\left| \sigma_{\text{est}}^2 - \left( \frac{\sum_i^N \mathbf{y}[i]^2 - \sum_i^N \mathbf{x}_q[i]^2}{N} \right) \right| < \epsilon, \quad (6)$$

where  $\mathbf{y}[i]$  and  $\mathbf{x}_q[i]$  show observed noisy and denoised signals by the filter with parameter  $q$ , respectively.  $\epsilon$  is a small value defining a stopping criterion for the optimization process. In 3DPBS, the selected filter realizes that the power of noise is equal to the power lost by the selected filter. Since 3DPBS allows floating-point for  $q$ , a polynomial approximation is required to calculate (5).

Unlike 3DPBS, an integer value  $q$  that minimizes (6) is selected in FGBD. Thus, (5) is simply calculated on the vertex domain which means that (5) can be directly calculated by

matrix operations. While this simplification reduces processing time, the denoising accuracy is sometimes degraded. To compensate for the quality of denoising, we propose an accurate filter selection method called FSLR. The filter selection method shown by (6) is based on the assumption that high-frequency components contain only noise. However, there are some cases in which the optimum filter is not selected because high-frequency components include sharply changing edges in original signals. The filter selection proposed in [14] utilizes all the points for the calculation of (6). In contrast, some points in a point cloud are selected to calculate (6) in FSLR. When (6) is calculated to decide the filter parameter  $q$ , we avoid utilizing the points that satisfy the following condition:  $(\sigma_R(i) + \sigma_G(i) + \sigma_B(i))/3 > 2\sigma_{\text{est}}$  where  $\sigma_R(i)$ ,  $\sigma_G(i)$ , and  $\sigma_B(i)$  indicate the standard deviations of red, green, and blue components in a patch  $\mathbf{a}_i$ , respectively. To choose a more suitable low-pass filter, the point whose patch has a large color variance far exceeding the noise level is not used for filter selection.

### 3. EXPERIMENTS

#### 3.1. Experimental conditions

**Datasets:** We evaluated all the frames in the 8iVFBv2 [17] and Microsoft voxelized upper bodies (MVUB) [18] datasets containing 1,200 and 1,202 frames. Their color signals  $\mathbf{f}_i$  were perturbed by additive Gaussian noise with standard deviation  $\sigma = 10, 20, \text{ or } 30$ .

**Evaluation metrics:** Peak signal-to-noise ratio (PSNR) was measured in the same way as the previous study [12]. To calculate the PSNR of the datasets [17, 18], we averaged each frame’s PSNR.

**Computer specifications:** For measuring processing time, the computer which has Intel Core i9-9900K CPU @ 3.60GHz, NVIDIA RTX 2070, and 64GB RAM was utilized.

#### 3.2. Experimental results

**(1) Processing time of FGBD:** First, we measured the processing time of each process of FGBD, and compared it with that of 3DPBS [14]. Since we implemented 3DPBS on a CPU, we prepared not only GPU implementation (FGBD-GPU) but also CPU implementation of FGBD (FGBD-CPU) for a fair comparison. Table 1 shows that FGBD can reduce the processing time from 3DPBS in all the processes. Although GPU implementation is effective in accelerating the processing, even in the comparison between 3DPBS and FGBD-CPU, FGBD-CPU is much faster than 3DPBS. Thus, the proposed algorithms were effective in accelerating denoising.

**(2) Comparison with conventional color denoising methods:** We compared FGBD with the conventional methods: GLR [12], CD-SGW [13], and 3DPBS [14]. In this experiment, noise estimation of FGBD was performed once every

**Table 2:** The PSNRs [dB] of denoised point clouds and the processing time [s] calculated by the conventional and proposed methods.

Dataset	$\sigma$	Noisy PSNR	GLR [12]		CD-SGW [13]		3DPBS[14]		FGBD-GPU	
			PSNR	Time	PSNR	Time	PSNR	Time	PSNR	Time
8iVFBv2 [17]	10	28.145	33.848	6.618	31.547	22.305	<b>35.003</b>	97.283	34.731	<b>0.021</b>
	20	22.175	30.921	7.199	29.538	21.620	<b>32.344</b>	88.505	31.772	<b>0.024</b>
	30	18.765	28.599	6.847	28.943	21.387	<b>30.533</b>	90.031	29.784	<b>0.024</b>
MVUB [18]	10	28.758	33.667	2.417	32.274	8.261	34.181	36.247	<b>34.765</b>	<b>0.010</b>
	20	23.045	30.379	2.832	28.059	8.314	29.789	34.248	<b>31.220</b>	<b>0.011</b>
	30	19.773	27.865	3.510	26.486	8.435	26.667	48.587	<b>28.683</b>	<b>0.012</b>

**Table 3:** Processing time comparison of the graph construction methods with the 8iVFBv2 dataset. The figures indicate the average processing time per frame [s] in the graph construction process.

Method	BF-KNN [21]	kdtree [23]	LBVH [24]	SLG
8iVFBv2	339.069	0.595	0.528	<b>0.008</b>
MUVB	43.883	0.226	0.200	<b>0.005</b>

**Table 4:** Comparison of the noise estimation error  $E_{ne} = |\sigma_{est} - \sigma_{act}|$  and processing time with the 8iVFBv2 dataset.

Noise level		$\sigma = 10$	$\sigma = 20$	$\sigma = 30$
MEGW [13]	Error $E_{ne}$	1.894	1.854	1.051
	Time [s]	15.112	18.651	18.263
NE-GBP w/o sort	Error $E_{ne}$	1.992	1.123	0.606
	Time [s]	<b>0.026</b>	<b>0.028</b>	<b>0.035</b>
NE-GBP	Error $E_{ne}$	<b>0.706</b>	<b>0.369</b>	<b>0.225</b>
	Time [s]	0.028	0.030	0.037

10 frames. In the other frames,  $q$  of the previous frame is utilized to accelerate the processing. Table 2 shows the quality of denoised point clouds and the processing time. Besides, Fig. 4 shows denoised point clouds for the 1st frame of the “david” sequence in the MVUB dataset [18]. According to Table 2 and Fig. 4, the denoising accuracy of FGBD is comparable to those of the state-of-the-art denoising methods. Besides, the processing time of FGBD is faster than 30fps with both datasets.

**(3) Comparison with other graph construction methods:** We compared the processing time of SLG and the conventional fast graph constructions, Brute-force KNN (BF-KNN) [21], kdtree [23] and LBVH [24]. BF-KNN, LBVH, and SLG are implemented on a GPU. Table 3 shows that SLG outperformed the conventional methods in terms of computational complexity.

**(4) Evaluation of NE-GBP:** We compared NE-GBP with the conventional noise level estimation method for point clouds called median estimator with graph wavelets (MEGW) [13] adopted in 3DPBS [14]. Table 4 shows the comparison results of the noise estimation error  $E_{ne} = |\sigma_{est} - \sigma_{act}|$  and processing time. Here,  $\sigma_{act}$  is the actual noise level. As described in Section 2.3, the order of points in a patch is explicitly defined in NE-GBP. To verify the importance of using a distance-based order, we compared our approach with a NE-

**Table 5:** The results of the ablation study of FSLR.

Dataset	FGBD (Full)		FGBD w/o FSLR	
	PSNR [dB]	Time [s]	PSNR [dB]	Time [s]
8iVFBv2	32.095	0.023	31.691	0.021
MVUB	31.556	0.011	31.112	0.010

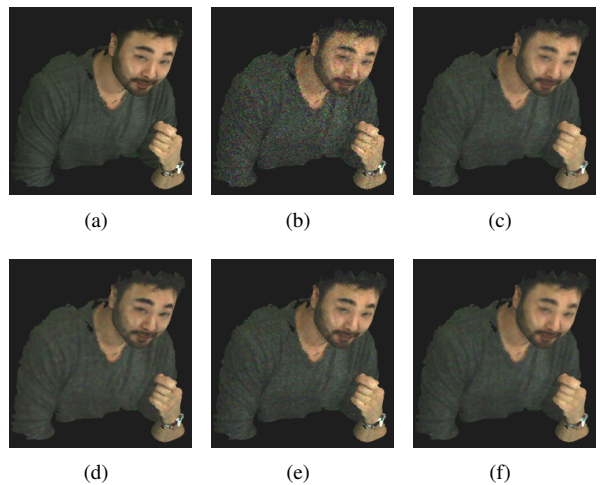


**Fig. 4:** The 1st frame of the “david” sequence in the MVUB with  $\sigma = 30$ : (a) ground truth, (b) noisy point cloud, denoising results by (c) GLR [12], (d) CD-SGW [13], (e) 3DPBS [14], and (f) FGBD.

GBP where the entries of the vector corresponding to each patch are not sorted (“NE-GBP w/o sort” in Table 4). According to Table 4, the error and processing time of NE-GBP are smaller than those of MEGW [13], and the order of points is important to acquire accurate noise levels. In addition, when we used “NE-GBP w/o sort” for denoising, there was a 0.4 dB deterioration (average of all the point clouds and noise levels) compared with the PSNR of FGBD introduced in Table 2.

**(5) Ablation study of FSLR:** To verify the effect of FSLR introduced in Section 2.4, we compared the full FGBD introduced in Table 2 to FGBD without FSLR. Table 5 shows the comparison results for each dataset where we averaged the PSNR and processing time for all noise levels. We observed an improvement of approximately 0.5dB for both datasets with a slight increase in processing time.

## 4. CONCLUSION

In this paper, we proposed a fast and accurate graph-based denoising method (FGBD). Our three proposals, a scan line graph (SLG), noise estimation using graph-based patches (NE-GBP), and filter selection with limited region (FSLR), lead to real-time denoising with a single GPU while maintaining accuracy. In the future, we will verify the effectiveness of FGBD not only for color signals but also for coordinate signals to enlarge the scope of FGBD.

## 5. REFERENCES

- [1] Gerd Bruder, Frank Steinicke, and Andreas Nüchter, “Immersive point cloud virtual environments,” in *2014 IEEE Symposium on 3D User Interfaces (3DUI)*, 2014, pp. 161–162.
- [2] Mostafa Agour and Thomas Kreis, “Experimental investigation of holographic 3D-TV approach,” in *2009 3DTV Conference: The True Vision - Capture, Transmission and Display of 3D Video*, 2009, pp. 1–4.
- [3] Bin Yang, Wenjie Luo, and Raquel Urtasun, “Pixor: Real-time 3D object detection from point clouds,” in *2018 IEEE/CVF Conference on Computer Vision and Pattern Recognition*, 2018, pp. 7652–7660.
- [4] Xing Li, Qian Huang, Tianjin Yang, and Qianhan Wu, “Hyperpointnet for point cloud sequence-based 3D human action recognition,” in *2022 IEEE International Conference on Multimedia and Expo (ICME)*, 2022, pp. 1–6.
- [5] Sebastian Schwarz, Marius Preda, Vittorio Baroncini, Madhukar Budagavi, Pablo Cesar, Philip A. Chou, Robert A. Cohen, Maja Krivokuća, Sébastien Lasserre, Zhu Li, Joan Llach, Khaled Mammou, Rufael Mekuria, Ohji Nakagami, Ernestasia Siahaan, Ali Tabatabai, Alexis M. Tourapis, and Vladyslav Zakharchenko, “Emerging MPEG standards for point cloud compression,” *IEEE Journal on Emerging and Selected Topics in Circuits and Systems*, vol. 9, no. 1, pp. 133–148, 2019.
- [6] Francesca Pistilli, Giulia Fracastoro, Diego Valsesia, and Enrico Magli, “Learning graph-convolutional representations for point cloud denoising,” in *The European Conference on Computer Vision (ECCV)*, 2020, pp. 103–118.
- [7] Shitong Luo and Wei Hu, “Differentiable manifold reconstruction for point cloud denoising,” in *The 28th ACM International Conference on Multimedia*, 2020, pp. 1330–1338.
- [8] Yann Schoenenberger, Johan Paratte, and Pierre Vandergheynst, “Graph-based denoising for time-varying point clouds,” in *2015 3DTV-Conference: The True Vision - Capture, Transmission and Display of 3D Video*, 2015, pp. 1–4.
- [9] Xianz Gao, Wei Hu, and Zongming Guo, “Graph-based point cloud denoising,” in *2018 IEEE Fourth International Conference on Multimedia Big Data (BigMM)*, 2018, pp. 1–6.
- [10] Dingkun Zhu, Honghua Chen, Weiming Wang, Haoran Xie, Gary Cheng, Mingqiang Wei, Jun Wang, and Fu Lee Wang, “Nonlocal low-rank point cloud denoising for 3-D measurement surfaces,” *IEEE Transactions on Instrumentation and Measurement*, vol. 71, pp. 1–14, 2022.
- [11] Xihua Sheng, Li Li, Dong Liu, and Zhiwei Xiong, “Attribute artifacts removal for geometry-based point cloud compression,” *IEEE Transactions on Image Processing*, vol. 31, pp. 3399–3413, 2022.
- [12] Chinthaka Dinesh, Gene Cheung, and Ivan V. Bajić, “3D point cloud color denoising using convex graph-signal smoothness priors,” in *2019 IEEE 21st International Workshop on Multimedia Signal Processing (MMSP)*, 2019, pp. 1–6.
- [13] Muhammad Abeer Irfan and Enrico Magli, “Joint geometry and color point cloud denoising based on graph wavelets,” *IEEE Access*, vol. 9, pp. 21149–21166, 2021.
- [14] Ryosuke Watanabe, Keisuke Nonaka, Eduardo Pavez, Tatsuya Kobayashi, and Antonio Ortega, “Graph-based point cloud color denoising with 3-dimensional patch-based similarity,” in *ICASSP 2023 - 2023 IEEE International Conference on Acoustics, Speech and Signal Processing (ICASSP)*, 2023, pp. 1–5.
- [15] Haoran Hong, Eduardo Pavez, Antonio Ortega, Ryosuke Watanabe, and Keisuke Nonaka, “Motion estimation and filtering for the inter prediction of dynamic point cloud compression,” in *2022 Picture Coding Symposium*, 2022.
- [16] S.G. Chang, Bin Yu, and M. Vetterli, “Adaptive wavelet thresholding for image denoising and compression,” *IEEE Transactions on Image Processing*, vol. 9, no. 9, pp. 1532–1546, 2000.
- [17] Eugene d’Eon, Bob Harrison, Taos Myers, and Philip A. Chou, “8i voxelized full bodies - a voxelized point cloud dataset,” in *ISO/IEC JTC1/SC29 Joint WG11/WG1 (MPEG/JPEG) input document WG11M40059/WG11M74006*, 2017.
- [18] C. Loop, Q. Cai, S. O. Escolano, and P. A. Chou, “Microsoft voxelized upper bodies - a voxelized point cloud dataset,” *ISO/IEC JTC1/SC29 Joint WG11/WG1 (MPEG/JPEG) input document m38673/M72012*, 2016.
- [19] Xueyi Wang, “A fast exact k-nearest neighbors algorithm for high dimensional search using k-means clustering and triangle inequality,” in *The 2011 International Joint Conference on Neural Networks*, 2011, pp. 1293–1299.
- [20] K G Renga Bashyam and Sathish Vadhiyar, “Fast scalable approximate nearest neighbor search for high-dimensional data,” in *2020 IEEE International Conference on Cluster Computing (CLUSTER)*, 2020, pp. 294–302.
- [21] Shengren Li and Nina Amenta, “Brute-force k-nearest neighbors search on the GPU,” in *Similarity Search and Applications*, Giuseppe Amato, Richard Connor, Fabrizio Falchi, and Claudio Gennaro, Eds., Cham, 2015, pp. 259–270, Springer International Publishing.
- [22] Vincent Garcia, Eric Debreuve, and Michel Barlaud, “Fast k nearest neighbor search using GPU,” in *2008 IEEE Computer Society Conference on Computer Vision and Pattern Recognition Workshops*, 2008, pp. 1–6.
- [23] Deyuan Qiu, Stefan May, and Andreas Nüchter, “GPU-accelerated nearest neighbor search for 3D registration,” in *Computer Vision Systems*, Mario Fritz, Bernt Schiele, and Justus H. Piater, Eds., Berlin, Heidelberg, 2009, pp. 194–203, Springer Berlin Heidelberg.
- [24] J. Jakob and M. Guthe, “Optimizing LBVH-construction and hierarchy-traversal to accelerate kNN queries on point clouds

- using the GPU,” *Computer Graphics Forum*, vol. 40, no. 1, pp. 124–137, 2021.
- [25] Linh Ha, Jens Krueger, and Claudio T. Silva, “Fast Four-Way Parallel Radix Sorting on GPUs,” *Computer Graphics Forum*, 2009.
- [26] Xinhao Liu, Masayuki Tanaka, and Masatoshi Okutomi, “Single-image noise level estimation for blind denoising,” *IEEE Transactions on Image Processing*, vol. 22, no. 12, pp. 5226–5237, 2013.
- [27] Guangyong Chen, Fengyuan Zhu, and Pheng Ann Heng, “An efficient statistical method for image noise level estimation,” in *2015 IEEE International Conference on Computer Vision (ICCV)*, 2015, pp. 477–485.
- [28] Rui Chen, Fei Zhao, Changshui Yang, Yuan Li, and Tiejun Huang, “Robust estimation for image noise based on eigenvalue distributions of large sample covariance matrices,” *Journal of Visual Communication and Image Representation*, vol. 63, pp. 102604, 2019.